Electronic Supplementary Material (ESI) for Sustainable Energy & Fuels.

Supporting Information

Pore-edge graphitic-nitride dominant hierarchically porous carbon for boosting oxygen reduction catalysis

Density functional theory (DFT) calculations

All models are calculated using Vienna ab-initio simulation package (VASP) with density-functional theory (DFT), and the Perdew-Burke-Ernzerhof (PBE) function within the generalized gradient approximation was applied by the exchange-correlation energy in the paper. The layer of graphene 6×6 sheet as the model of graphene and the vacuum space above these sheets were taken to be 18 Å. The convergence criteria for energy and force during the optimization process are 0.01 eV/Å and 10^{-5} eV, respectively. The cutoff energy and K-point were set to 500 eV and 5×5×1, respectively. The spin polarization is considered throughout the calculations. Applying semi empirical dispersion correction density functional theory (DFT-D3) to correct the van der Waals interaction forces between molecules and catalysts. The adsorption energy (E_{ads}) of ORR intermediates is calculated as follows:

$$E_{ads} = E_{total} - E_o - E_{sub}$$

where the E_{total} is total adsorption energy of the catalyst and species, E_{sub} is the catalyst energy without adsorption, and E_o is the energy of the species.The pathways on N-C systems were calculated in detail according to electrochemical framework developed by Nørskov. The freeenergy change of every elementary reaction is calculated as follows:

$$\Delta G = \Delta E + \Delta ZPE - T\Delta S + \Delta G_{field} + \Delta G_U + \Delta G_{pH}$$

Where ΔE is the reaction energy change, T is the temperature (289.15 K), ΔS is the vibrational entropy change, and ΔZPE is the zero point energy, respectively. The parameters of ΔZPE and ΔS can be calculated according to the vibration frequency of oxygen-contained intermediates. The influence of electric potential on the Gibbs free energy is expressed by ΔG_U=-neU, where n is the number of electrons transferred and U is the electrode potential. In this study, ΔG_{pH} and ΔG_{field} are not involved because they have less contribution to the trends of free energy change.

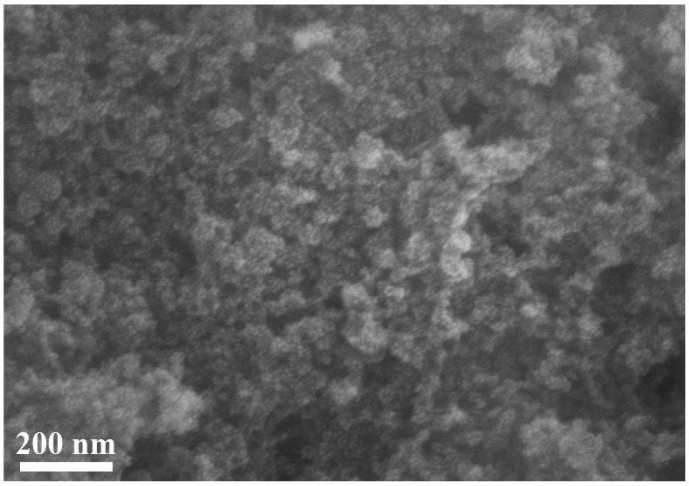

Figure S1. SEM image of nano-SiO_2.

Figure S2. SEM images of N-C bulk (without SiO_2 template-assisted growth).

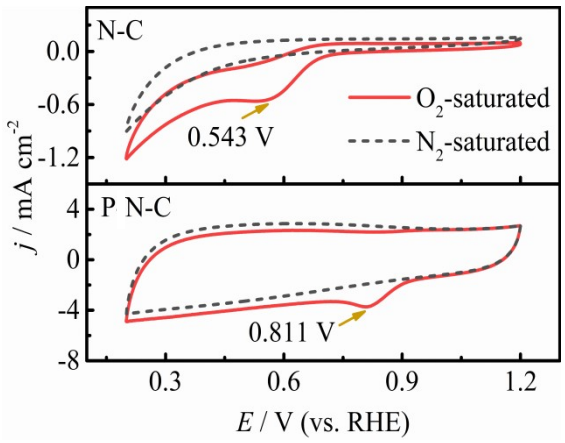

Figure S3. Cyclic voltammetry of N-C and P N-C in N_2 or O_2 saturated 0.1 M KOH solution.

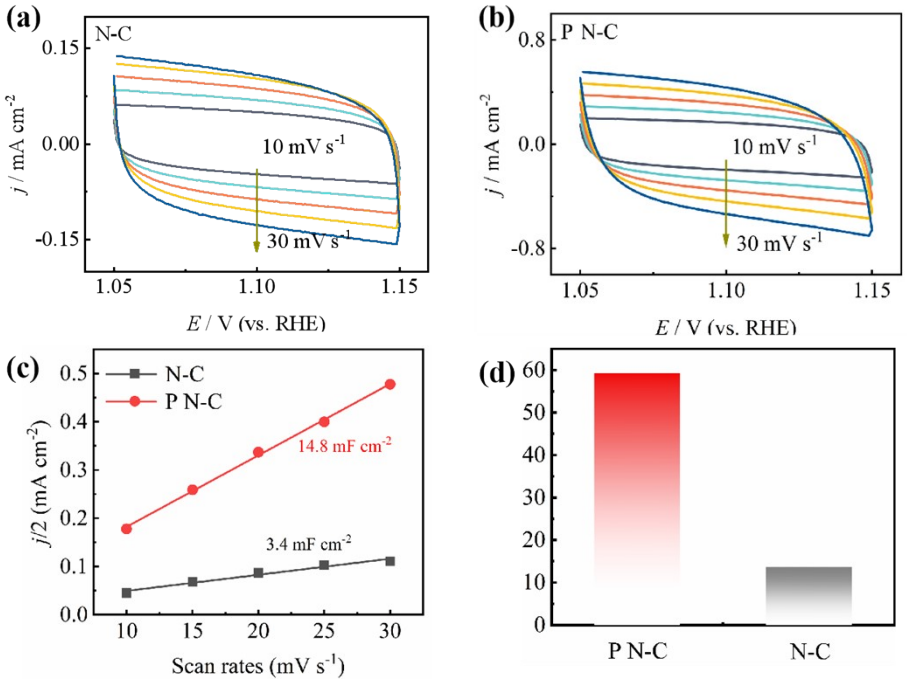

Figure S4. (a-c) CV curves with different scan rates and the corresponding normalized C_{dl} results of P N-C and N-C, respectively. (d) Calculated ECAS results.

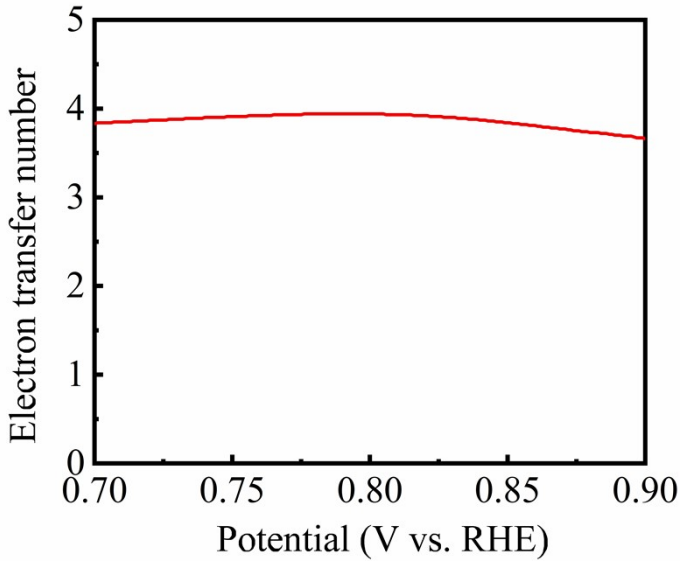

Figure S5 The electron transfer number of P N-C catalyst calculated by RRDE result.

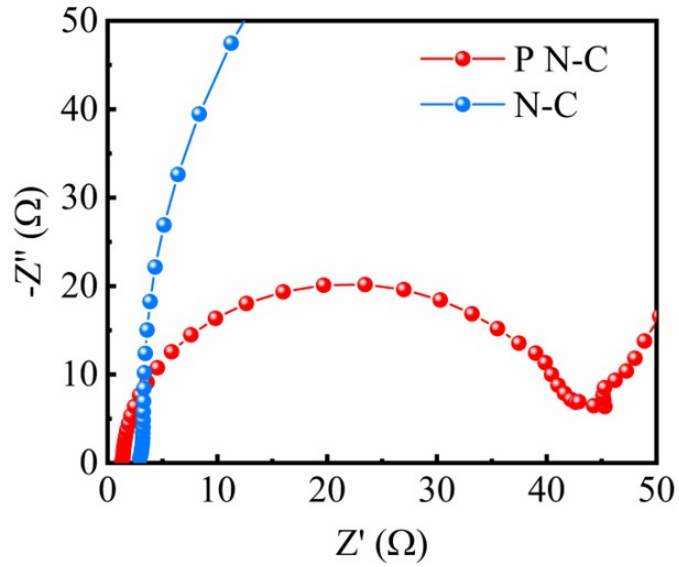

Figure S6. EIS curves of P N-C and N-C.

Figure S6. Contact angle results of N-C and P N-C, respectively.

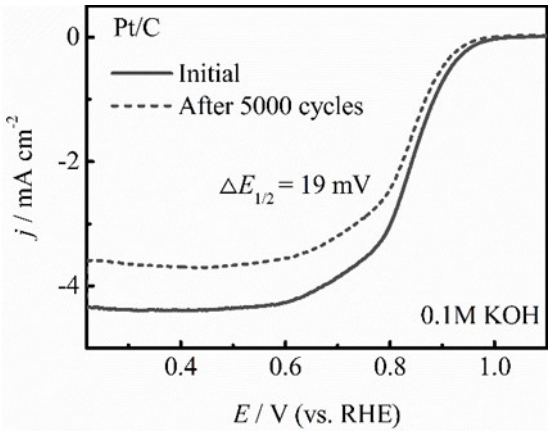

Figure S7. Pt/C ORR polarisation curves before and after 5000 potential cycles.

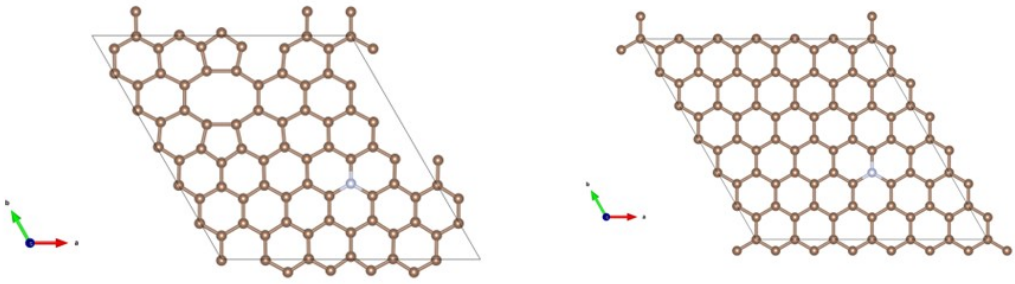

Figure S8. The optimized calculation models of pore-edged N-C and bulk N-C, respectively.

Table S1. Specific surface area and pore parameters of as-prepared materials.

Catalysts	Specific surface area (m^2 g^{-1})	Micropore area (m^2 g^{-1})	Pore volume (cm^3 g^{-1})	Average pore diameter (nm)
N-C	14.9	27.7564	0.0143	3.2716
P N-C	847.8	290.1971	2.157088	10.1773

Table S2. The content of C, N, O of the prepared catalysts obtained from XPS

Catalysts (at%)	C	N	O
N-C	90.3	4.43	5.27
P N-C	85.55	2.24	12.21

Table S3. EIS-fitting results of the prepared catalysts

	Rs	Rct	CPE1-T	CPE1-P
N-C	1.337	42.53	$2.41E^{-5}$	0.978
P N-C	2.849	258.7	$6.892E^{-6}$	0.982

Table S4. A comparison table of the ORR performance between this work and recently reported Pt-free catalysts in alkaline and acidic medium (vs. RHE)

Materials	$E_{1/2}$ (V) in 0.1 M KOH	References
P N-C	0.842	This work
$CoC_x/(Co_{0.55}Fe_{1.945})2P@C$	0.840	[1]
$Co_6Mo_6C_2$-Co@NC	0.803	[2]
$Mn_{0.9}Fe_{2.1}C/NC$	0.780	[3]
Fe_2Ni_2N/Co@ NCNT	0.760	[4]
Ni_3FeN/Co,N-CNF	0.810	[5]

CoN_x/NGA	0.830	[6]
$Ni_{2.25}Co_{0.75}N$/NrGO-3	0.790	[7]
Fe–CNSs–N	0.84	[8]
Fe_3C–FeN/NC	0.8	[9]
FeN_4CB	0.81	[10]
Co-MOF-T	0.84	[11]
Co_p@CoNC	0.84	[12]
FeN_4–SC–NiN_4	0.84	[13]
$NiFe_3$@NGHS	0.84	[14]
FeNi/N–LCN	0.84	[15]
$FeNi_3$/NC	0.79	[16]
CoFe/S–NC	0.84	[17]
FeCo/NSC	0.82	[18]
CoN_4–HPC	0.78	[19]
CoNi/N–CNN	0.82	[20]
Fe/Ni@NiCo–CNT	0.8	[21]
$(Fe, Co, Ni)_9S_8$/NSCFs	0.82	[22]
FeCoNi–N–rGO	0.84	[23]
CoFeNi@CNT	0.82	[24]

Reference

1. Wu, Y., et al., *The cobalt carbide/bimetallic CoFe phosphide dispersed on carbon nanospheres as advanced bifunctional electrocatalysts for the ORR, OER, and rechargeable Zn–air batteries.* Journal of Colloid and Interface Science, 2021. **590**: p. 321-329.
2. Li, Y., et al., *Bimetallic cobalt molybdenum carbide–cobalt composites as superior bifunctional oxygen electrocatalysts for Zn–air batteries.* Materials Today Energy, 2020. **18**.
3. Lin, C., et al., *Long-Life Rechargeable Zn Air Battery Based on Binary Metal Carbide Armored by Nitrogen-Doped Carbon.* ACS Applied Energy Materials, 2019. **2**(3): p. 1747-1755.
4. Wu, M., et al., *Ultra-long life rechargeable zinc-air battery based on high-performance trimetallic nitride and NCNT hybrid bifunctional electrocatalysts.* Nano Energy, 2019. **61**: p. 86-95.
5. Wang, Q., et al., *3D carbon nanoframe scaffold-immobilized Ni3FeN nanoparticle electrocatalysts for rechargeable zinc-air batteries' cathodes.*

Nano Energy, 2017. **40**: p. 382-389.
6. Zou, H., et al., *In situ coupled amorphous cobalt nitride with nitrogen-doped graphene aerogel as a trifunctional electrocatalyst towards Zn-air battery deriven full water splitting.* Applied Catalysis B: Environmental, 2019. **259**.
7. He, Y., et al., *Hybrid Nanostructures of Bimetallic NiCo Nitride/N-Doped Reduced Graphene Oxide as Efficient Bifunctional Electrocatalysts for Rechargeable Zn–Air Batteries.* ACS Sustainable Chemistry & Engineering, 2019. **7**(24): p. 19612-19620.
8. Wang, Y., et al., *Fe3O4/Fe2O3/Fe nanoparticles anchored on N-doped hierarchically porous carbon nanospheres as a high-efficiency ORR electrocatalyst for rechargeable Zn–air batteries.* Journal of Materials Chemistry A, 2021. **9**(5): p. 2764-2774.
9. Zhou, F., et al., *The cooperation of Fe3C nanoparticles with isolated single iron atoms to boost the oxygen reduction reaction for Zn–air batteries.* Journal of Materials Chemistry A, 2021. **9**(11): p. 6831-6840.
10. Zhao, X., et al., *Boron modulating electronic structure of FeN4C to initiate high-efficiency oxygen reduction reaction and high-performance zinc-air battery.* Journal of Energy Chemistry, 2022. **66**: p. 514-524.
11. Duan, X., et al., *MOF-derived Co-MOF,O-doped carbon as trifunctional electrocatalysts to enable highly efficient Zn–air batteries and water-splitting.* Journal of Energy Chemistry, 2021. **56**: p. 290-298.
12. Yang, H., et al., *Designing superior bifunctional electrocatalyst with high-purity pyrrole-type CoN4 and adjacent metallic cobalt sites for rechargeable Zn-air batteries.* Energy Storage Materials, 2022. **46**: p. 553-562.
13. Su, K., et al., *Customizing the anisotropic electronic states of janus-distributive FeN4 and NiN4 dual-atom sites for reversible oxygen electrocatalysis.* Applied Catalysis B: Environmental, 2023. **331**.
14. Ma, Y., et al., *NiFe nanoparticles supported on N-doped graphene hollow spheres entangled with self-grown N-doped carbon nanotubes for liquid electrolyte/flexible all-solid-state rechargeable zinc–air batteries.* Journal of Materials Chemistry A, 2022. **10**(23): p. 12616-12631.
15. Li, X., et al., *Rechargeable Zn–Air Batteries with Outstanding Cycling Stability Enabled by Ultrafine FeNi Nanoparticles-Encapsulated N-Doped Carbon Nanosheets as a Bifunctional Electrocatalyst.* Nano Letters, 2021. **21**(7): p. 3098-3105.
16. Chen, K., et al., *Enhancing ORR/OER active sites through lattice distortion of Fe-enriched FeNi3 intermetallic nanoparticles doped N-doped carbon for high-performance rechargeable Zn-air battery.* Journal of Colloid and Interface Science, 2021. **582**: p. 977-990.
17. Li, G., et al., *S, N co-doped carbon nanotubes coupled with CoFe nanoparticles as an efficient bifunctional ORR/OER electrocatalyst for rechargeable Zn-air batteries.* Chemical Engineering Journal, 2022. **429**.
18. Chang, S., H. Zhang, and Z. Zhang, *FeCo alloy/N, S dual-doped carbon composite as a high-performance bifunctional catalyst in an advanced*

rechargeable zinc-air battery. Journal of Energy Chemistry, 2021. **56**: p. 64-71.
19. Liu, Y., et al., *CoNi nanoalloy-Co-N4 composite active sites embedded in hierarchical porous carbon as bi-functional catalysts for flexible Zn-air battery.* Nano Energy, 2022. **99**.
20. Li, J., et al., *In-situ growth of CoNi bimetal anchored on carbon nanoparticle/nanotube hybrid for boosting rechargeable Zn-air battery.* Journal of Energy Chemistry, 2022. **66**: p. 348-355.
21. Ma, M., et al., *Low-temperature liquid reflux synthesis of core@shell structured Ni@Fe-doped NiCo nanoparticles decorated on carbon nanotubes as a bifunctional electrocatalyst for Zn–air batteries.* Journal of Materials Chemistry A, 2022. **10**(24): p. 13088-13096.
22. Jiang, T., et al., *Fish bone-derived N, S co-doped interconnected carbon nanofibers network coupled with (Fe, Co, Ni)9S8 nanoparticles as efficient bifunctional electrocatalysts for rechargeable and flexible all-solid-state Zn-air battery.* Electrochimica Acta, 2021. **373**.
23. Chen, X., et al., *A hierarchical architecture of Fe/Co/Ni-doped carbon nanotubes/nanospheres grafted on graphene as advanced bifunctional electrocatalyst for Zn-Air batteries.* Journal of Alloys and Compounds, 2021. **873**.
24. Chen, D., et al., *Developing nitrogen and Co/Fe/Ni multi-doped carbon nanotubes as high-performance bifunctional catalyst for rechargeable zinc-air battery.* Journal of Colloid and Interface Science, 2021. **593**: p. 204-213.